

Angular dependence of the topological Hall effect in the uniaxial van der Waals ferromagnet Fe_3GeTe_2

Yurong You,¹ Yuanyuan Gong,¹ Hang Li,² Zefang Li,² Mengmei Zhu,¹ Jiaxuan Tang,¹ Enke Liu,² Yuan Yao,² Guizhou Xu,^{1,*} Feng Xu,^{1,†} and Wenhong Wang²

¹*School of Materials Science and Engineering, Nanjing University of Science and Technology, Nanjing 210094, China*

²*State Key Laboratory for Magnetism, Beijing National Laboratory for Condensed Matter Physics, Institute of Physics, Chinese Academy of Sciences, Beijing 100190, China*



(Received 22 July 2019; published 31 October 2019)

Fe_3GeTe_2 is a paradigmatic two-dimensional ferromagnet with strong uniaxial anisotropy. In this work we systematically studied the angular dependence of electrical transport properties in Fe_3GeTe_2 single crystals, and uncovered an unexpected topological Hall effect (THE) in the configuration of large tilted magnetic fields. The Hall resistivity and magnetoresistance varied periodically when the external magnetic field rotated in the ac (or bc) plane, while the THE emerged and maintained robust with fields swept across the nearby hard-magnetized ab plane. The approximate in-plane THE covered the whole temperature region below T_C (~ 150 K) and reached the maximum value at 100 K. Emergence of an internal gauge field was proposed to explain the origin of this large THE, which is generated by either the possible topological domain structure of uniaxial Fe_3GeTe_2 or the noncoplanar spin structure forming during the in-plane magnetization. Our results promise to provide an alternative detection method to the in-plane skyrmion formation and may bring a brand new prospective to magnetotransport studies in condensed matter physics.

DOI: [10.1103/PhysRevB.100.134441](https://doi.org/10.1103/PhysRevB.100.134441)

I. INTRODUCTION

Emergent electromagnetism [1] induced by the internal gauge field has triggered many novel and interesting transport phenomena, for instance, the unusual large anomalous Hall effect (AHE) in noncollinear antiferromagnets [2–4] or contributed by topological Weyl or nodal line band structure [5,6]. On the other hand, topological Hall effect (THE) is also uncovered in systems with scalar spin chirality [7,8] or topological spin texture [9–11] (skyrmions, typically). These Berry-phase driven phenomena have deeply enriched our understanding of the fundamental physics of magnetotransport, especially the Hall effect, as well as offered versatile options to spintronic applications [3,6].

A regular Hall effect is measured during the applied magnetic field (\mathbf{H}), the electrical current (\mathbf{I}), and the measured voltage (\mathbf{V}) are mutually vertical. There exists a so-called planar Hall effect (PHE) [12], where the Hall signal is otherwise obtained in the plane parallel to \mathbf{H} . The PHE results from neither of the mechanisms accounting for AHE, but actually relates to the anisotropic magnetoresistance (AMR) [13,14]. A giant PHE has been reported in the ferromagnetic semiconductor films [15] and recently in the topological Weyl semimetals that correlate with chiral anomaly [16,17]. However, the essence of the PHE makes it exhibit symmetric curves while sweeping \mathbf{H} , as observed in most cases [15,18], rather than an antisymmetric one like a normal Hall effect. In addition, the transverse voltage will vanish when \mathbf{I} is perpendicular or parallel to \mathbf{H} according to its phenomenological

expression (will be discussed later). But there are several works reporting the AHE-like signal in a PHE configuration [19,20], which are currently explained by either a high-order contribution or noncollinear spin structure.

Here we studied the angular dependence of the Hall effect in a quasi-two-dimensional van der Waals ferromagnet Fe_3GeTe_2 [21], and identified an uncommon THE emerging when \mathbf{H} rotated away from its usual perpendicular direction. It should be noted that Wang *et al.* [22] have already reported a similar-shape THE in Fe_3GeTe_2 , but the conventional three-axis configuration was applied there, making it different from the phenomenon observed here. The observed THE was proposed to be originated from the emergent gauge field that associates with the possible topological or chiral spin structure of Fe_3GeTe_2 . Our results can potentially provide an effective method to detect the in-plane topological spin texture, particularly in a two-dimensional (2D) system and further extend the understanding of the Hall effect and may bring a new prospective to magnetotransport studies in condensed matter physics.

II. EXPERIMENTAL DETAILS

High-quality single crystals were grown through the self-flux method from a mixture of pure elements Fe (99.8%), Ge (99.9999%), and Te (99.99%) with a composition of Fe_2GeTe_4 [23]. The mixture was then sealed in an evacuated quartz tube and heated to 1233 K. The melt was held at 1233 K for 12 h, then cooled slowly to 948 K with a rate of 3 K/h, and finally cooled down to room temperature. The typical size of the single crystals is $\sim 2 \times 2 \times 0.1$ mm, with a cleavable layer in the ab plane. The crystal structure was identified by x-ray diffraction (XRD, Bruker D8 Advance)

*Corresponding author: gzxu@njjust.edu.cn

†Corresponding author: xufeng@njjust.edu.cn

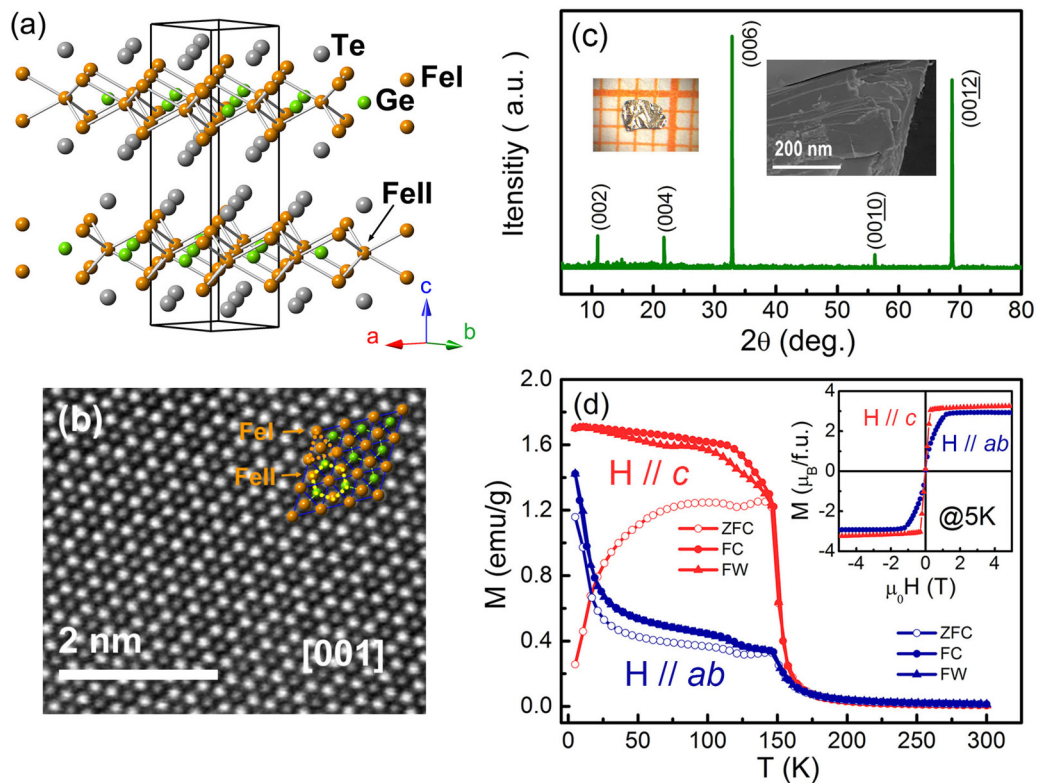


FIG. 1. Structure and magnetic properties of the single crystal Fe_3GeTe_2 . (a) Schematic of the hexagonal structure of Fe_3GeTe_2 (space group $P6_3/mmc$). (b) High-resolution STEM image taken from the [001] axis. The inset shows the arrangement of the triangular structure of Fe_I atoms and the hexagonal ring of Fe_{II} -Ge layer. (c) XRD pattern for the as-grown slice of Fe_3GeTe_2 single crystal. The optical photograph and SEM image in the inset shows the typical size and stepped like appearance of the sample. (d) Temperature dependence of the ZFC, FC, and FW magnetization measured at $\mu_0 H = 0.01$ T for $\mathbf{H} // ab$ and $\mathbf{H} // c$. Inset shows the anisotropic M - H curve at $T = 5$ K.

with $\text{Cu-K}\alpha$ radiation. The element composition and atomic configuration were examined by energy-dispersive spectroscopy (EDS) in the scanning electron microscope (SEM, FEI Quanta 250F) and high-resolution scanning transmission electron microscopy (STEM, JEOL ARM200F), respectively. The atomic ratio determined by EDS is $\sim 3 : 1 : 2.2$, exhibiting slightly off-stoichiometric, which may account for the lowering Curie temperature of our samples compared to the ones grown by the chemical vapor transport (CVT) [24–26]. Magnetization and transport properties were measured in the superconducting quantum interference device (SQUID) and Physical Property Measurement System (PPMS, Quantum Design), respectively. For transport measurements, the samples were cut into regular rectangle shape and a six-probe method was applied to simultaneously measure the magnetoresistance (MR) and Hall resistivity. The final MR and Hall data were symmetrized to exclude the misalignment of the electrode.

III. RESULTS AND DISCUSSIONS

Fe_3GeTe_2 is a van der Waals ferromagnet that crystallizes in space group $P6_3/mmc$ with a layered Fe_3Ge substructure sandwiched by two Te layers [21]. As shown in Fig. 1(a), the Fe_3Ge substructure contains two inequivalent Fe_I and Fe_{II} atoms, contributing to a Fe_{II} -Ge hexagonal atomic ring layer and two separated triangular lattice Fe_I - Fe_I layers. The

hexagonal ring was clearly resolved in the high-resolution STEM image in Fig. 1(b), which also confirmed the stacked structure and high quality of our samples. Typical XRD pattern of the as-grown sample in Fig. 1(c) verified the expected single-crystalline nature, with all the reflections along the crystallographic orientation [001].

The temperature dependence of magnetization under zero-field cooled (ZFC), field cooled (FC), and field warming (FW) are measured with $\mu_0 H = 0.01$ T, both in parallel and perpendicular to the c axis, as seen in Fig. 1(d). A ferromagnetic transition is observed at approximately 150 K for both directions, similar to that reported for the flux-grown samples [23,27,28]. The ZFC and FC curves show obvious splitting in $\mathbf{H} // c$ below T_C like other typical frustrated ferromagnets [11,29,30], and the difference in magnitude for the two directions indicates the anisotropic character of the low-temperature magnetic phase. A slight kink at about 125 K below T_C is also observed, consistent with the possible two-stage magnetic ordering transition [26]. The magnetization curves at 5 K for both $\mathbf{H} // c$ and $\mathbf{H} // ab$ directions distinctly demonstrate the strong magnetocrystalline anisotropy in Fe_3GeTe_2 with the easy axis along the c direction. The saturated magnetic moment (M_S) is $3.25 \mu_B/\text{f.u.}$ for $\mathbf{H} // c$, also consistent with the reported values [21–23].

The magnetotransport properties for \mathbf{H} perpendicular to the current plane have been previously investigated [6,22], and a large anomalous Hall current has been identified in the

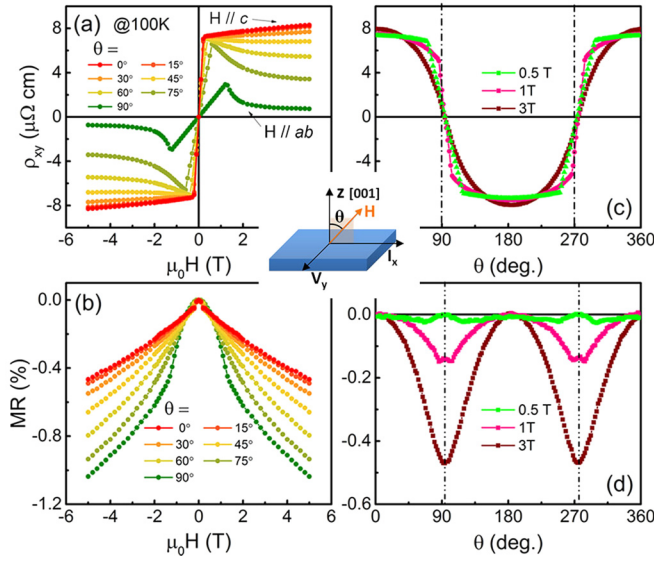


FIG. 2. Separate (a) $\rho_{xy}(H)$ and (b) MR curves measured in the ab plane with \mathbf{H} in the direction of $\theta = 0^\circ, 15^\circ, 30^\circ, 45^\circ, 60^\circ, 75^\circ,$ and 90° at 100 K. The angular dependence of (c) ρ_{xy} and (d) MR at 100 K under the field of 0.5, 1, and 3 T. In the middle it shows the schematic of the measurement configuration.

ab plane owing to the topological nodal line band structure [6]. In this work, first we measured ρ_{xy} and ρ_{xx} in the ab plane while gradually rotating the \mathbf{H} in the ac (or bc) plane, that is, from the usual c axis to the ab plane, as shown in the middle schematic of Fig. 2. We define the angle between the external magnetic field and the normal of the sample plane as θ . When $\theta = 0^\circ$, large anomalous Hall resistivity and Hall angle are reproduced in our samples (see the Supplemental Material Fig. S1 [31]), consistent with that previously reported [6]. With θ increasing from 0° to 90° , we find that ρ_{xy} gradually reduces, while a pronounced cusplike anomaly arises in the low field region of the curve and becomes rather distinct for $\theta = 90^\circ$, as shown in Fig. 2(a). But it should be mentioned that there can be discrepancy between the measured and actual angle of \mathbf{H} and \mathbf{I} . The full angular dependence of ρ_{xy} in Fig. 2(c) further reveals this deviation, where all curves merge to zero at a degree that is slightly higher ($< 5^\circ$) than 90° or 270° . To track the exact in-plane situation, detailed $\rho_{xy}(H)$ around $\theta = 90^\circ$ are investigated in a much smaller interval (of $\sim 2^\circ$), as shown in the Supplemental Material Fig. S2 [31]. It can be seen that there actually exists a specific angle near 90° (here about 93°) in which the THE is almost completely vanished. This means that the THE in the strict in-plane setup does not exist. However, it emerges and grows rapidly in a rather small region around the in-plane direction, and can be detected most times by measuring the nominal in-plane ρ_{xy} (see the Supplemental Material Fig. S3 [31] for another two samples). Simultaneously, a clear bend at the same field where the THE emerges is observed in the MR curves in Fig. 2(b). We proposed that this near in-plane Hall and MR anomaly could result from an internal field that pointed in the perpendicular direction, which will be elaborated on later.

The angular dependence of ρ_{xy} is expected to follow a $\cos\theta$ relation in a normal situation, as the AHE scales with the

out-of-plane component of \mathbf{H} [32]. Hence the AHE component at $\theta = 90^\circ$ or 270° in Fig. 2(c) is anticipated to vanish, but there remains small values in the figure, which are caused by the above mentioned misalignment error. It is noted here only at $\mu_0H = 3$ T that the curve accords with a smooth periodic relation (approaching $\cos\theta$), while at $\mu_0H = 0.5$ and 1 T, on account of the existence of the large THE, it deviates and presents a sharp sign reverse across the 90° or 270° . The angular dependent MR in Fig. 2(d) showed a twofold pattern peaking around 90° (270°), with anisotropy of $\sim -0.5\%$ [$= (\rho_{//} - \rho_{\perp})/\rho_{\perp}$] under a field of 3 T.

Furthermore, to establish a clearer picture of the abnormal THE, we measured the in-plane Hall resistivity ρ_{xy} and MR at various temperatures from 5 to 170 K when $\theta = 90^\circ$, i.e., in the vicinity of \mathbf{H}/\mathbf{I} , as shown in Figs. 3(a) and 3(b). The cusp in ρ_{xy} is highest at $T = 100$ K and persists all temperatures below T_C in the low field region. The MR curves are all negative while a bend or upturn emerges at lower temperature. Here the in-plane Hall data were disposed in the same process as that in normal mutual-vertical configuration. The THE contribution is denoted as ρ_{xy}^T , thus the total Hall resistivity $\rho_{xy} = \mu_0 R_0 H + R_S M + \rho_{xy}^T$, where the first two terms represent the ordinary and anomalous Hall contribution, respectively. As the MR is overall less than 1%, R_S can be simplified as $S_A \rho_{xx}^2$, in which S_A is field independent and ρ_{xx} is the longitudinal resistivity [10,33]. ρ_{xy}^T is thus extracted in combination with the in-plane M - H curves (misalignment is ignored here), as shown representatively in Fig. 3(c), which also demonstrates that the peak of ρ_{xy} just appears at the anisotropy field of the M - H curve. By extracting ρ_{xy}^T over the temperature range of 5–170 K, we constitute the phase diagram in Fig. 3(d) by contour mapping in the temperature and magnetic field plane. In general, the near in-plane THE exists from 0.3 to 1.5 T, and covers the whole temperature below T_C . A maximum value of $2.04 \mu\Omega \text{ cm}$ is obtained at 100 K in Fe_3GeTe_2 single crystal, which is quite large and nearly more than ten times of those observed in systems containing skyrmion phase [9,11,34]. But it should be noted this value may be not the maximum among all the tilted angles, as the THE distinctly exists in a range of about 15° around the in-plane direction, as seen in Fig. 2(a) and Fig. S2.

Finally, we measured the angular dependence of ρ_{xy} and MR with the field rotated in the ab plane at 100 K to examine the in-plane anisotropy. Due to the possible misalignment, the magnetic field may not be located in the exact ab plane and the rotation axis may not be strictly along c axis. The angle between \mathbf{H} and \mathbf{I} in the ab plane is denoted as φ . It can be seen in Figs. 4(a) and 4(b) that the THE can be altered substantially by the change of φ , while the MR shows slight increase with invariable shape. By sweeping φ in the positive ($+H$) and negative field ($-H$), we obtain two curves of $\rho_{xy}(\varphi)$ which are actually not superposed (not shown), demonstrating again the existence of a large antisymmetric THE. The angular dependence of ρ_{xy} extracted by $[\rho_{xy}(+H) - \rho_{xy}(-H)]/2$, as shown in the inset of Fig. 4(a), is well-described by the $\sin\varphi$ formulation. The largest magnitude is presented at $H = 1$ T, where the THE dominates. But it should be noted that the evolution of planar ρ_{xy} with φ is not fixed. Our measurements of several samples present varying tendency upon φ changing, despite that they all follow a rough $\sin(\varphi + x)$ relation (Supplemental

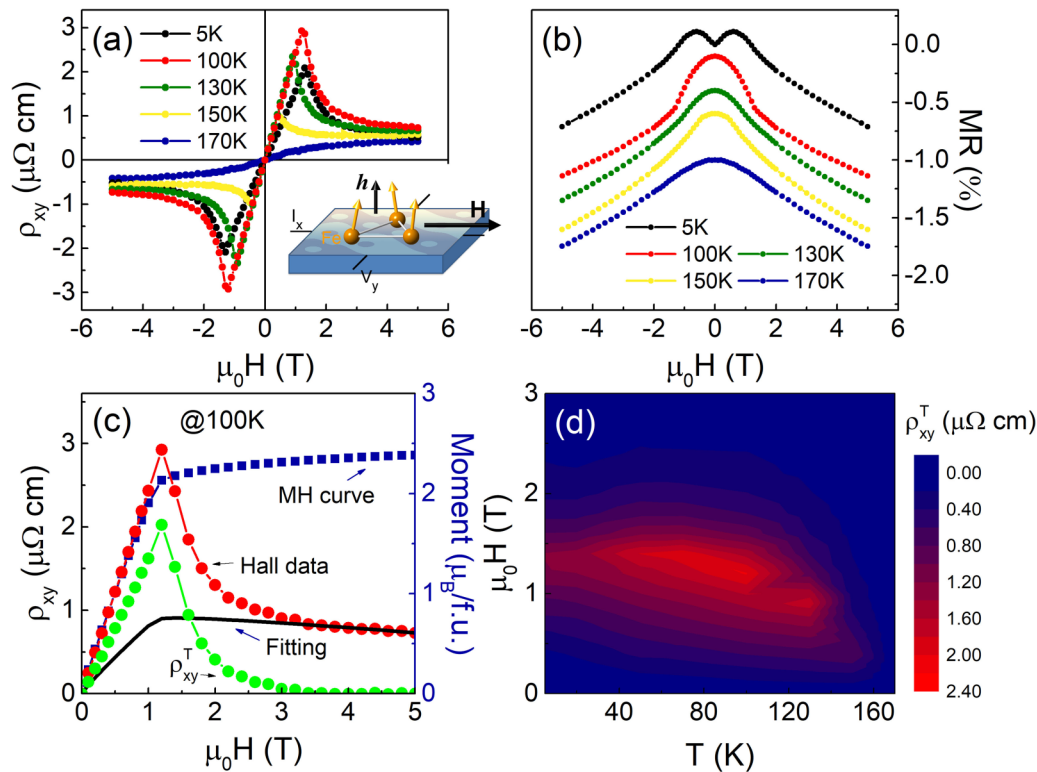


FIG. 3. In-plane (a) ρ_{xy} and (b) MR of Fe_3GeTe_2 single crystal at various temperatures for $\mathbf{H} \parallel \mathbf{I}$ (which is not strict considering the misalignment, see the text). Inset is the configuration of the measurement, as well as the schematic of the possible origin that generated an inside gauge field of \mathbf{h} . (c) The representative ρ_{xy} curve (red) and in-plane M - H curve (blue) measured at 100 K, calculated $R_0 B + S_A \rho_{xx}^2 M$ fitting curve (black) and extracted ρ_{xy}^T curve (green). (d) The contour mapping of extracted ρ_{xy}^T as a function of the external magnetic field and temperature.

Material Figs. S4(a)–S4(c) [31]). Therefore, the largest THE is not always observed at $\mathbf{H} \parallel \mathbf{I}$, neither at $\mathbf{H} \perp \mathbf{I}$. Considering the misalignment mentioned above, an out-of-plane component of ρ_{xy} can exist and is rather stochastic when making different measurements, thus possibly causing a random phase shift to the $\sin\varphi$ relationship. Another possibility would be related to the specific crystal direction in the ab plane, which deserves further investigation. The PHE in Fig. 4(c) is obtained by $[\rho_{xy}(+H) + \rho_{xy}(-H)]/2$, and to eliminate the possible in-plane AMR contribution resulting from the misalignment of the Hall electrodes, the procedure of $[\rho_{xy}(\varphi) - \rho_{xy}(\pi - \varphi)]/2$ is also applied [35,36]. The extracted $\rho_{xy}^{\text{PHE}}(\varphi)$ roughly follows $\rho_{xy}^{\text{PHE}} = (\rho_{\parallel} - \rho_{\perp}) \sin\varphi \cos\varphi$, where ρ_{\parallel} and ρ_{\perp} are the resistivity when \mathbf{H} is applied parallel or perpendicular to \mathbf{I} , similar to the reported behavior [18,32]. Hence, the variation of ρ_{xy}^{PHE} mainly depends on the magnitude of AMR [expressed as $(\rho_{\parallel} - \rho_{\perp})/\rho_{\perp}$], as shown in Fig. 4(d) [37]. Finally, it should be mentioned that an out-of-plane longitudinal MR may also be caused by the oblique of the sample and exhibit a $\cos^2(\varphi + \delta)$ dependence, where δ is stochastic [35]. However, we find that despite the planar ρ_{xy} displaying a rather random phase shift as mentioned above, the $\rho_{xy}^{\text{PHE}}(\varphi)$ stably follows the $\sin 2\varphi$ relation, as seen in the Supplemental Material Figs. S4(d)–S4(f) [31]. Therefore, the influence of the out-of-plane MR can be ignored in our samples and the PHE is thought to be intrinsic here. Both the magnitude of the

PHE and AMR is rather small, implying the weak in-plane anisotropy in this uniaxial van der Waals ferromagnet.

Furthermore, from the expression of ρ_{xy}^{PHE} , it can be seen that planar ρ_{xy}^{PHE} will vanish when \mathbf{I} is perpendicular or parallel to \mathbf{H} ($\varphi = 0$ or $\pi/2$), and will exhibit a symmetric relationship to \mathbf{H} instead of an antisymmetric one like a conventional Hall effect [15,18]. There are some examples where a small AHE-like signal is observed [19,20], which are currently explained by a high-order contribution or noncollinear spin structure. But the large presence of THE in the almost in-plane is a phenomenon that is first identified. Since there is nearly no external perpendicular component of the magnetic field in this configuration, we refer to the possible internal gauge field that accounts for the extra enhancement of ρ_{xy} . On one hand, we notice that the topological (bubblelike) domain structure in the ab plane of Fe_3GeTe_2 has been suspected by the previous MFM and STM measurements [38,39]. Moreover, during the submission of this paper, observation of the topological chiral magnetic skyrmions in the ab plane is reported in the arXiv by Park *et al.* [40]. Our recent experimental progress also revealed the presence of skyrmion bubbles in Fe_3GeTe_2 single crystal (not published). Therefore, we reasonably speculate that the in-plane topological spin texture gives rise to an internal gauge field \mathbf{h} that finally results in the appearance of THE in the inclined magnetic fields, as schematically depicted in the inset of Fig. 3(a). This just resembles the widely

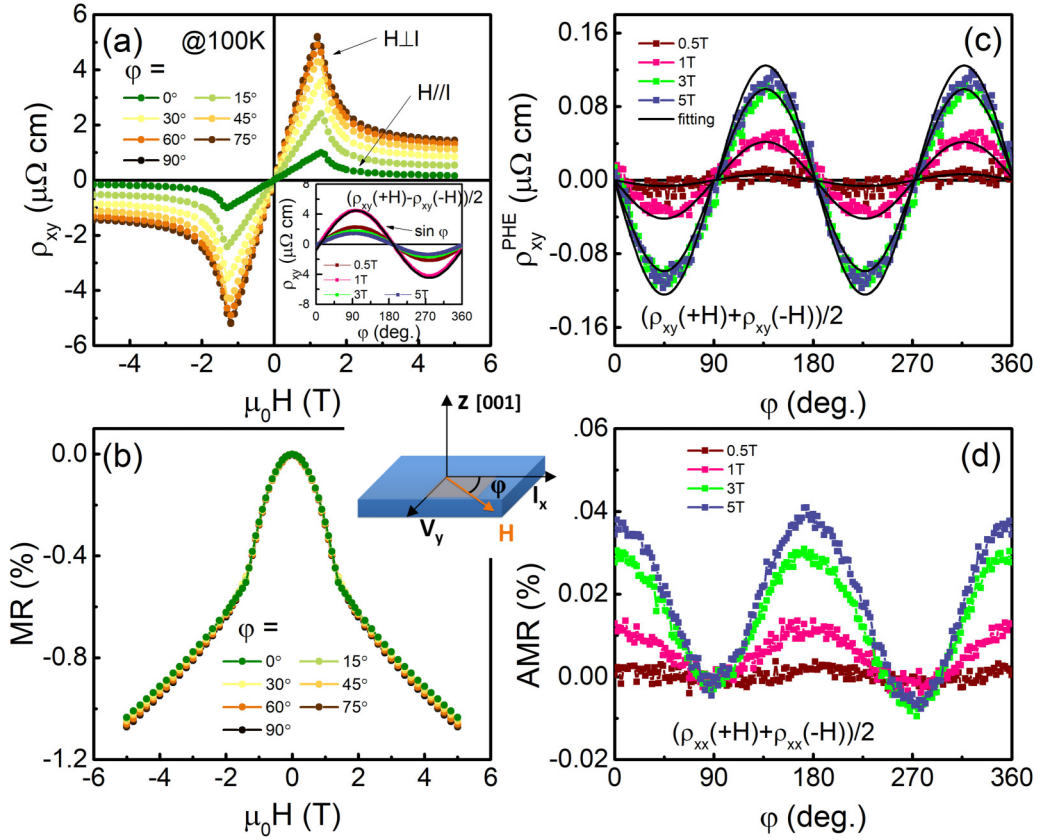


FIG. 4. Magnetic field dependence of in-plane (a) ρ_{xy} and (b) MR at $\phi = 0^\circ, 15^\circ, 30^\circ, 45^\circ, 60^\circ, 75^\circ$, and 90° at 100 K. The inset in (a) is the angular dependence of ρ_{xy} by subtracting the original curve in positive and negative field $[\rho_{xy}(+H) - \rho_{xy}(-H)]/2$. The angular dependence of the (c) planar Hall ρ_{xy}^{PHE} , obtained by $[\rho_{xy}(+H) + \rho_{xy}(-H)]/2$, and further symmetrized by $[\rho_{xy}(\phi) - \rho_{xy}(\pi - \phi)]/2$, and (d) AMR at 100 K under the field of 0.5, 1, 3, and 5 T.

studied THE in the conventional configuration [9–11,41]. The biggest difference is that here the ρ_{xy}^T only appears in the largely oblique field, which may indicate the occurrence of some topological transformation modulated by the direction of the external field. Notably, the almost completely exclusion of AHE in the pristine THE makes it an efficient detection method of in-plane skyrmion formation [42]. On the other hand, nonvanishing spin chirality associated with noncoplanar spin structure can induce a similar gauge field [1,22]. As proved by our experiments as well as the literature [22,24], Fe_3GeTe_2 is a strong uniaxial magnet with easy axis along the c direction (out-of-plane), and meanwhile the Fe atoms form a rather frustrated triangular structure (as seen in Fig. 1). Hence, during the in-plane magnetization process, the spins of Fe atoms could form a noncoplanar structure that contributes to the \mathbf{h} [also schematically shown in inset of Fig. 3(a)], where further evidence is still needed. These are the two possibilities that can generate an internal field to arouse the THE in large tilted magnetic fields.

IV. CONCLUSIONS

In summary, by three-dimensional rotation of the magnetic field with respect to the sample plane, we have observed a large topological Hall effect when the external field tilted

to the hard magnetized but easily cleavable ab plane in the van der Waals ferromagnet Fe_3GeTe_2 . Systematic studies on the angular dependence reveal the dynamical evolution of the Hall resistivity and MR in both the ac and ab plane. The THE nearby the ab plane exists in the whole temperature region below T_C and a maximum value of $2.04 \mu\Omega$ cm is observed at 100 K, which is much larger than those observed in most skyrmion systems. We attribute the origin of this THE to the emergence of a gauge field, which is very likely to be a result of the reported topological domain structure of the uniaxial Fe_3GeTe_2 . The THE in this new configuration can provide an alternative way to detect in-plane skyrmion formation, particularly in the natural two-dimensional system and thin films, where the Hall effect on other sides are hardly accessible.

ACKNOWLEDGMENTS

This work is supported by National Natural Science Foundation of China (Grants No. 11604148, No. 51601092, and No. 11874410), the National Key R&D Program of China (Grant No. 2017YFA0303202), and the Fundamental Research Funds for the Central Universities (Grant No. 30919012108).

- [1] N. Nagaosa and Y. Tokura, *Phys. Scr.* **T146**, 014020 (2012).
- [2] H. Chen, Q. Niu, and A. H. MacDonald, *Phys. Rev. Lett.* **112**, 017205 (2014).
- [3] S. Nakatsuji, N. Kiyohara, and T. Higo, *Nature (London)* **527**, 212 (2015).
- [4] A. K. Nayak, J. E. Fischer, Y. Sun, B. Yan, J. Karel, A. C. Komarek, C. Shekhar, N. Kumar, W. Schnelle, J. Kübler, C. Felser, and S. S. P. Parkin, *Sci. Adv.* **2**, e1501870 (2016).
- [5] E. Liu, Y. Sun, N. Kumar, L. Muechler, A. Sun, L. Jiao, S. Yang, D. Liu, A. Liang, Q. Xu, J. Kroder, V. Süß, H. Borrmann, C. Shekhar, Z. Wang, C. Xi, W. Wang, W. Schnelle, S. Wirth, Y. Chen, S. T. B. Goennenwein, and C. Felser, *Nat. Phys.* **14**, 1125 (2018).
- [6] K. Kim, J. Seo, E. Lee, K.-T. Ko, B. S. Kim, B. G. Jang, J. M. Ok, J. Lee, Y. J. Jo, W. Kang, J. H. Shim, C. Kim, H. W. Yeom, B. I. Min, B.-J. Yang, and J. S. Kim, *Nat. Mater.* **17**, 794 (2018).
- [7] Y. Taguchi, Y. Oohara, H. Yoshizawa, N. Nagaosa, and Y. Tokura, *Science* **291**, 2573 (2001).
- [8] Y. Machida, S. Nakatsuji, Y. Maeno, T. Tayama, T. Sakakibara, and S. Onoda, *Phys. Rev. Lett.* **98**, 057203 (2007).
- [9] N. Kanazawa, Y. Onose, T. Arima, D. Okuyama, K. Ohoyama, S. Wakimoto, K. Kakurai, S. Ishiwata, and Y. Tokura, *Phys. Rev. Lett.* **106**, 156603 (2011).
- [10] S. X. Huang and C. L. Chien, *Phys. Rev. Lett.* **108**, 267201 (2012).
- [11] W. Wang, Y. Zhang, G. Xu, L. Peng, B. Ding, Y. Wang, Z. Hou, X. Zhang, X. Li, E. Liu, S. Wang, J. Cai, F. Wang, J. Li, F. Hu, G. Wu, B. Shen, and X.-X. Zhang, *Adv. Mater.* **28**, 6887 (2016).
- [12] J. P. Pan, in *Solid State Physics*, edited by F. Seitz and D. Turnbull (Academic, New York, 1957), Vol. 5, pp. 1–96.
- [13] Z. Q. Lu, G. Pan, and W. Y. Lai, *J. Appl. Phys.* **90**, 1414 (2001).
- [14] K. M. Seemann, F. Freimuth, H. Zhang, S. Blügel, Y. Mokrousov, D. E. Bürgler, and C. M. Schneider, *Phys. Rev. Lett.* **107**, 086603 (2011).
- [15] H. X. Tang, R. K. Kawakami, D. D. Awschalom, and M. L. Roukes, *Phys. Rev. Lett.* **90**, 107201 (2003).
- [16] A. A. Burkov, *Phys. Rev. B* **96**, 041110(R) (2017).
- [17] S. Nandy, G. Sharma, A. Taraphder, and S. Tewari, *Phys. Rev. Lett.* **119**, 176804 (2017).
- [18] H. Li, H.W. Wang, H. He, J. Wang, and S.Q. Shen, *Phys. Rev. B* **97**, 201110(R) (2018).
- [19] P. K. Muduli, K.-J. Friedland, J. Herfort, H.-P. Schönherr, and K. H. Ploog, *Phys. Rev. B* **72**, 104430 (2005).
- [20] Y. You, X. Chen, X. Zhou, Y. Gu, R. Zhang, F. Pan, and C. Song, *Adv. Electron. Mater.* **5**, 1800818 (2019).
- [21] H.-J. Deiseroth, K. Aleksandrov, C. Reiner, L. Kienle, and R. K. Kremer, *Eur. J. Inorg. Chem.* **2006**, 1561 (2006).
- [22] Y. Wang, C. Xian, J. Wang, B. Liu, L. Ling, L. Zhang, L. Cao, Z. Qu, and Y. Xiong, *Phys. Rev. B* **96**, 134428 (2017).
- [23] A. F. May, S. Calder, C. Cantoni, H. Cao, and M. A. McGuire, *Phys. Rev. B* **93**, 014411 (2016).
- [24] B. Chen, J. Yang, H. Wang, M. Imai, H. Ohta, C. Michioka, K. Yoshimura, and M. Fang, *J. Phys. Soc. Jpn.* **82**, 124711 (2013).
- [25] V. Y. Verchenko, A. A. Tsirlin, A. V. Sobolev, I. A. Presniakov, and A. V. Shevelkov, *Inorg. Chem.* **54**, 8598 (2015).
- [26] J. Yi, H. Zhuang, Q. Zou, Z. Wu, G. Cao, S. Tang, S. A. Calder, P. R. C. Kent, D. Mandrus, and Z. Gai, *2D Mater.* **4**, 011005 (2016).
- [27] Y. Liu, E. Stavitski, K. Attenkofer, and C. Petrovic, *Phys. Rev. B* **97**, 165415 (2018).
- [28] Y. Liu, V. N. Ivanovski, and C. Petrovic, *Phys. Rev. B* **96**, 144429 (2017).
- [29] Z. Hou, W. Ren, B. Ding, G. Xu, Y. Wang, B. Yang, Q. Zhang, Y. Zhang, E. Liu, F. Xu, W. Wang, G. Wu, X. Zhang, B. Shen, and Z. Zhang, *Adv. Mater.* **29**, 1701144 (2017).
- [30] Z. Hou, Q. Zhang, G. Xu, S. Zhang, C. Gong, B. Ding, H. Li, F. Xu, Y. Yao, E. Liu, G. Wu, X.-X. Zhang, and W. Wang, *ACS Nano* **13**, 922 (2019).
- [31] See Supplemental Material at <http://link.aps.org/supplemental/10.1103/PhysRevB.100.134441> for Fig. S1 showing the Hall resistivity ρ_{xy} and MR at variable temperature when the magnetic field is applied along the c direction. Figure S2 shows $\rho_{xy}(H)$ curves measured in the ab plane with \mathbf{H} in the direction of $\theta = 80^\circ - 100^\circ$ with much smaller intervals at 100 K. Figure S3 shows the Hall and longitudinal resistivity for \mathbf{H}/\mathbf{I} at various temperatures for another two samples. Figure S4 shows the angular dependence of ρ_{xy} and ρ_{xy}^{PHE} of three other samples (S5–S7) at 100 K under various fields.
- [32] N. Kumar, S. N. Guin, C. Felser, and C. Shekhar, *Phys. Rev. B* **98**, 041103(R) (2018).
- [33] Y. Li, N. Kanazawa, X. Z. Yu, A. Tsukazaki, M. Kawasaki, M. Ichikawa, X. F. Jin, F. Kagawa, and Y. Tokura, *Phys. Rev. Lett.* **110**, 117202 (2013).
- [34] P. Sergelius, J. Gooth, S. Bäßler, R. Zierold, C. Wiegand, A. Niemann, H. Reith, C. Shekhar, C. Felser, B. Yan, and K. Nielsch, *Sci. Rep.* **6**, 33859 (2016).
- [35] Q. Liu, F. Fei, B. Chen, X. Bo, B. Wei, S. Zhang, M. Zhang, F. Xie, M. Naveed, X. Wan, F. Song, and B. Wang, *Phys. Rev. B* **99**, 155119 (2019).
- [36] D. Liang, Y. Wang, W. Zhen, J. Yang, S. Weng, X. Yan, Y. Han, W. Tong, W. Zhu, L. Pi, and C. Zhang, *AIP Adv.* **9**, 055015 (2019).
- [37] D. Thompson, L. Romankiw, and A. Mayadas, *IEEE Trans. Magn.* **11**, 1039 (1975).
- [38] N. León-Brit, E. D. Bauer, F. Ronning, J. D. Thompson, and R. Movshovich, *J. Appl. Phys.* **120**, 083903 (2016).
- [39] G. D. Nguyen, J. Lee, T. Berlijn, Q. Zou, S. M. Hus, J. Park, Z. Gai, C. Lee, and A. P. Li, *Phys. Rev. B* **97**, 014425 (2018).
- [40] T.-E. Park, L. Peng, J. Liang, A. Hallal, X. Zhang, S. J. Kim, K. M. Song, K. Kim, M. Weigand, G. Schuetz, S. Finizio, J. Raabe, J. Xia, Y. Zhou, M. Ezawa, X. Liu, J. Chang, H. C. Koo, Y. D. Kim, M. Chshiev, A. Fert, H. Yang, X. Yu, and S. Woo, [arXiv:1907.01425](https://arxiv.org/abs/1907.01425).
- [41] N. Nagaosa and Y. Tokura, *Nat. Nanotechnol.* **8**, 899 (2013).
- [42] T. Yokouchi, N. Kanazawa, A. Tsukazaki, Y. Kozuka, A. Kikkawa, Y. Taguchi, M. Kawasaki, M. Ichikawa, F. Kagawa, and Y. Tokura, *J. Phys. Soc. Jpn.* **84**, 104708 (2015).